114 *Biochemistry* **2010,** *49,* 114–123
DOI: 10.1021/bi901677z

BIOCHEMISTRY
including biophysical chemistry & molecular biology
Article

Role of the Glutamic Acid 54 Residue in Transthyretin Stability and Thyroxine Binding[†,‡]

Masanori Miyata,[§] Takashi Sato,[§] Mineyuki Mizuguchi,[#] Teruya Nakamura,[∥] Shinji Ikemizu,[∥] Yuko Nabeshima,[#] Seiko Susuki,[§] Yoshiaki Suwa,[⊥] Hiroshi Morioka,[⊥] Yukio Ando,[△] Mary Ann Suico,[§] Tsuyoshi Shuto,[§] Tomoaki Koga,[§] Yuriko Yamagata,*[,∥] and Hirofumi Kai*[,§]

[§]*Departments of Molecular Medicine, Global COE Cell Fate Regulation Research and Education Unit,* [∥]*Structural Biology, and* [⊥]*Analytical and Biophysical Chemistry, Graduate School of Pharmaceutical Sciences, Kumamoto University, 5-1 Oe-Honmachi, Kumamoto 862-0973, Japan,* [#]*Faculty of Pharmaceutical Sciences, University of Toyama, Toyama 930-0914, Japan, and* [△]*Department of Diagnostic Medicine, Graduate School of Medical Sciences, Kumamoto University, 1-1-1 Honjo, Kumamoto 860-0811, Japan*

Received September 25, 2009; Revised Manuscript Received November 30, 2009

ABSTRACT: Transthyretin (TTR) is a tetrameric protein associated with amyloidosis caused by tetramer dissociation and monomer misfolding. The structure of two TTR variants (E54G and E54K) with Glu54 point mutation that cause clinically aggressive amyloidosis remains unclear, although amyloidogenicity of artificial triple mutations (residues 53−55) in β-strand D had been investigated. Here we first analyzed the crystal structures and biochemical and biophysical properties of E54G and E54K TTRs. The direction of the Lys15 side chain in E54K TTR and the surface electrostatic potential in the edge region in both variants were different from those of wild-type TTR. The presence of Lys54 leads to destabilization of tetramer structure due to enhanced electrostatic repulsion between Lys15 of two monomers. Consistent with structural data, the biochemical analyses demonstrated that E54G and E54K TTRs were more unstable than wild-type TTR. Furthermore, the entrance of the thyroxine (T_4) binding pocket in TTR was markedly narrower in E54K TTR and wider in E54G TTR compared with wild-type TTR. The tetramer stabilization and amyloid fibril formation assays in the presence of T_4 showed lower tetramer stability and more fibril formation in E54K and E54G TTRs than in wild-type TTR, suggesting decreased T_4 binding to the TTR variants. These findings indicate that structural modification by Glu54 point mutation may sufficiently alter tetramer stability and T_4 binding.

Familial amyloid polyneuropathy (FAP) is a hereditary neurodegenerative disease caused by a point mutation in the human plasma protein transthyretin (TTR)[1] (*1*, *2*). TTR generated in the liver and choroid plexus is one of the three proteins in the extracellular fluid responsible for the distribution of thyroxine (T_4) (*3*−*5*). TTR forms a 55-kDa homotetramer composed of four identical 14-kDa monomers with 127 amino acid residues. TTR monomer is composed of eight β-strands, A through H, which form two four-strand (inner sheet DAGH and outer sheet CBEF) antiparallel β-sheets and a short α-helix. Two monomers form a dimer via a network of hydrogen bond interactions involving the two edge β-strands, H and F, and two dimers form a tetramer through hydrophobic and hydrogen bond interactions of AB and GH loops between two dimers (*6*−*11*). The tetramer of TTR has two T_4 binding pockets, which are involved in tetramer stability by binding with T_4 between two dimers (*12*−*14*).

Extensive biochemical and biophysical studies support the model that amyloid formation results from destabilization of the tetrameric quaternary structure of TTR, probably leading to the formation of an alternatively folded monomeric amyloidogenic intermediate, which may constitute the building block of amyloid (*15*). Therefore, small structural perturbation caused by point mutation possibly destabilizes the native quaternary and tertiary structures, enhancing amyloid fibril formation. More than 80 different point mutations are known to be associated with FAP, and amyloidogenicity of TTR variants differs with position of mutation. β-Strand D that is composed of Gly53, Glu54, and Leu55 is predicted to be a mutational hot spot (*16*). The artificial multiple mutations and deletions in β-strand D result in significant destabilization of the TTR fold and enhance amyloid fibril formation, corroborating the involvement of this region in the formation of the TTR amyloidogenic intermediate (*16*). Moreover, L55P TTR, a naturally occurring mutation, shows early onset, the most aggressive phenotype of FAP, and low kinetic and thermodynamic stabilities (*17*). X-ray crystallographic and NMR studies of L55P TTR demonstrated that the

[†]This work was supported by grants from the Amyloidosis Research Committee, the Pathogenesis and Therapy of Hereditary Neuropathy Research Committee, Surveys and Research on Specific Disease, the Ministry of Health and Welfare of Japan, the Charitable Trust Clinical Pathology Research Foundation of Japan, the Mochida Memorial Foundation for Medical and Pharmaceutical Research, and Grants-in-Aid for Scientific Research from the Ministry of Education, Sciences, Sports, and Culture (MEXT) of Japan and from the Global COE Program (Cell Fate Regulation Research and Education Unit), MEXT Japan.

[‡]The atomic coordinates and structure factors of wild-type TTR and Glu54 TTR variants have been deposited in the Protein Data Bank with the following accession numbers: for human wild-type TTR, 3A4D; for E54G TTR, 3A4E; for E54K TTR, 3A4F.

*To whom correspondence should be addressed. Telephone and Fax: (81)-96-371-4405 or (81)-96-371-4638. E-mail: hirokai@gpo.kumamoto-u.ac.jp or yamagata@gpo.kumamoto-u.ac.jp.

[1]Abbreviations: TTR, transthyretin; T4, thyroxine; ThT, thioflavin T; rmsd, root mean square deviation; WT, wild type.

 Published on Web 12/01/2009

structure of β-strand D is highly disordered because the hydrogen bond interaction between β-strands A and D is disrupted in this variant (*7*, *18*, *19*). Although the importance of β-strand D or Leu55 residue in amyloidogenesis is well studied, the role of Glu54 in TTR amyloidogenesis is less known. Considering that the mutation of the Glu54 residue is known to cause a clinically aggressive form of FAP (*20*−*23*), the Glu54 residue may play an important role in TTR protein stability.

It is now accepted that tetramer dissociation into monomer is the rate-limiting step for amyloid fibril formation (*24*). Therefore, small molecules that can bind to the T_4 binding pocket and stabilize the TTR tetramer have been developed as amyloid fibril inhibitors (*13*, *14*, *25*). Structural analysis of the TTR−T_4 complex revealed that T_4 binding to TTR creates a new hydrogen bond network that results in stabilizing the tetramer conformation and that some hydrophobic and hydrophilic residues are involved in T_4 binding to TTR (*12*, *26*). In particular, Glu54 and Lys15 residues, which provide polar interactions between alanyl moieties of T_4, have been suggested to be important for T_4 binding to TTR (*12*, *27*). However, there is yet no direct evidence about the role of Glu54 in T_4 binding using Glu54 TTR variants. Recently, we demonstrated using a cell culture system that the Glu54 TTR variant, E54K TTR, is not stabilized by T_4, unlike the wild-type TTR, V30M TTR, or L55P TTR (*28*). Because Glu54 is located at the entrance of T_4 binding pocket, we speculate that Glu54 is one of the crucial residues in stabilizing the quaternary structure of TTR by small molecules that can bind to the T_4 binding pocket.

In this study, we investigated in detail the role of the Glu54 residue in TTR tetramer stability and T_4 binding in structural, biochemical, and biophysical viewpoints using two Glu54 TTR variants, Glu54Gly (E54G) and Glu54Lys (E54K) TTRs, which have been reported to display aggressive phenotypes of FAP (*20*−*23*). The crystal structures of E54K and E54G TTRs revealed that the environment structure around β-strand D was altered. The direction of Lys15 side chain in E54K TTR and the surface electrostatic potential in the edge region in both variants were different from wild-type TTR. These structural changes enhanced the electrostatic repulsion between Lys15 of two monomers. Furthermore, the structure of the entrance of the T_4 binding pocket was markedly narrower in E54K and wider in E54G TTR compared with that of wild-type TTR due to the length of their side chains that consequently interfered with the action of T_4. Consistent with structural data, E54K TTR and, to a lesser extent, E54G TTR are resistant to the tetramer stabilizing effect of T_4 compared with wild-type TTR. These results suggest that the Glu54 residue plays important roles in tetramer stability by affecting surface electrostatic potential and in T_4 binding by affecting the T_4 binding pocket.

EXPERIMENTAL PROCEDURES

Expression and Purification of TTR in Escherichia coli. Expression plasmids for E54G TTR and E54K TTR were prepared using the QuickChange II XL site-directed mutagenesis kit from Stratagene (La Jolla, CA) with wild-type TTR as template. Human E54G TTR and E54K TTR were subcloned into the *Nde*I and *Sal*I sites of pET-22b (+) vector (Novagen), and the sequences of the inserted DNA segments were verified by DNA sequencing. E54G TTR and E54K TTR were expressed in *E. coli* BL21(DE3) using the pET-22b (+) system. When the OD_{600} of the *E. coli* cell culture reached approximately 0.6, protein expression was induced by the addition of isopropyl β-D-thiogalactopyranoside (IPTG) at a final concentration of 1 mM. Twenty-four hours after induction, cells were harvested by centrifugation. The cell pellets were resuspended in 20 mM phosphate (pH 7.0). After cell lysis by sonication, E54G TTR and E54K TTR were detected in the soluble fraction. Protein purification was performed by anion-exchange chromatography and reverse-phase high-performance liquid chromatography.

Circular Dichroism Spectra Measurement. Circular dichroism (CD) spectra were measured using a Jasco J-805 spectropolarimeter (Japan Spectroscopic Co., Ltd., Tokyo, Japan). The temperature of the measuring cell was maintained at 25 °C by circulating water. Quartz cuvettes with path lengths of 1 and 10 mm were used for the far- and near-UV CD measurements, respectively. The buffer solution contained 50 mM sodium phosphate, 100 mM KCl, and 1 mM ethylenediaminetetraacetic acid (EDTA) (pH 7.0). Protein concentrations of the samples for the CD spectra were 17−40 μM as determined by measuring the absorbance at 280 nm using an extinction coefficient (ε_{280}) of 18450 M^{-1} cm^{-1}. Samples for the urea-induced unfolding were prepared as described previously (*29*). Before CD measurements were performed, samples of wild-type TTR, E54G TTR, and E54K TTR were incubated in 0−8 M urea at 25 °C for 96 h. The protein concentrations of the samples for the urea-induced unfolding were 29−31 μM.

Acid-Induced Tetramer-to-Monomer Transition Assay. The fractions of tetramers and monomers were monitored by sodium dodecyl sulfate−polyacrylamide gel electrophoresis (SDS−PAGE) as described previously (*28*). Before applying them onto the SDS−PAGE gel, protein solutions (0.2 mg/mL) in 100 mM phosphate or 200 mM acetate buffer containing 100 mM KCl at pH 3.5−7.0 were incubated at 4 °C for 40 h. The protein solutions (10 μL) were mixed with 5 μL of gel-loading buffer containing 0.1% SDS and 13% glycerol. Nonboiled samples were loaded on a 15% SDS−acrylamide gel. Protein bands were visualized by Coomassie brilliant blue R-250. Fractions of monomers, dimers, and tetramers were quantified by densitometry using the program SCION IMAGE (Scion Corp., Frederick, MD)

Crystallization, Data Collection, and Structure Determination. Crystals suitable for X-ray diffraction were obtained by the sitting-drop vapor-diffusion method at 20 °C. Crystals were grown within 10 days by mixing 2 μL of the TTR with 2 μL of reservoir solution containing 200 mM citrate buffer and 3 M ammonium sulfate (pH 5.3). Crystals were transferred to reservoir solutions containing 30% (v/v) glycerol and frozen in liquid nitrogen. The X-ray diffraction data were collected at beamline BL17A (WT), BL5A (E54G), and NW12 (E54K) of Photon Factory. Diffraction data were processed and scaled with the HKL2000 program suite (*16*). All structures obtained by molecular replacement starting from the available high-resolution crystal structures of human TTR (PDB accession code 1BMZ (*30*)) were refined using the programs CNS (*31*) and COOT (*32*). To follow the progress of refinement, the R_{free} value was monitored from the beginning, with 5% of the reflections included in the test set. At the final stage refinements were performed with REFMAC (*33*) using the translation, libration, screw-rotation (TLS) method. All figures for the structures were drawn using PyMol (http://pymol.sourceforge.net). The surface electrostatic potential of TTRs was drawn using ccp4mg (*34*). The data collection and refinement statistics are summarized in Table 1.

Table 1: Structural Data and Refinement Statistics of Wild-Type TTR and Glu54 TTR Variants

	WT TTR	E54G TTR	E54K TTR
data collection			
space group	$P2_12_12$	$P2_12_12$	$P2_12_12$
cell dimensions			
a, *b*, *c* (Å)	85.840, 43.084, 64.290	85.671, 41.617, 63.239	86.203, 42.466, 64.012
α, *β*, *γ* (deg)	90, 90, 90	90, 90, 90	90, 90, 90
resolution range used in scaling (highest resolution shell)	50−2.0 (2.07−2.0)	50−1.70 (1.76−1.70)	50−1.99 (2.06−1.99)
no. of observations	110563 (10857)	175619 (12483)	116844 (11508)
no. of unique reflections	16752 (1645)	24735 (2190)	16692 (1644)
completeness (%)	99.9 (100)	97.0(87.1)	99.6 (100)
$I/\sigma(I)$	36.2 (8.53)	52.3 (6.5)	45.6 (11.1)
R_{merge} (%)[a]	9.5 (33.6)	4.3 (21.9)	6.4 (21.0)
refinement			
resolution range used in refinement (Å)	33.0−2.0	31.6−1.7	35.8−1.99
no. of reflections in working set	15872	23436	15800
no. of reflections in test set	846	1265	842
atoms	1947	1981	1951
R-factor for working set (%)[b]	16.8	20.0	17.2
R_{free} for test set (%)[c]	22.9	23.8	22.3
rmsd bond length (Å)	0.026	0.022	0.024
rmsd bond angles (deg)	2.068	2.041	2.158
mean *B* value (Å^2)	17.559	23.960	27.415
residue range (A, B)	10−125, 10−124	10−125, 10−124	10−125, 10−124

[a] $R_{merge} = \sum_h\sum_i|I_{ih} - \langle I_h\rangle|/\sum_h\sum_i\langle I_h\rangle|$, where $\langle I_h\rangle$ is the mean intensity of the *i* observations over all reflections *h*. [b] *R*-factor $= \sum||F_o| - |F_c||/\sum|F_o|$, where $|F_o|$ and $|F_c|$ are the observed and calculated structure factor amplitudes, respectively. [c] R_{free} = as for *R*-factor but calculated for a test set comprising reflections not used in refinement.

TTR Stabilization Assay. The TTR stabilization assay was performed as described previously (*28*). Briefly, Chinese hamster ovary (CHO-K1) cells grown on six-well plates in Dulbecco's modified Eagle's medium supplemented with 10% fetal bovine serum were transfected with 2 μg of pEF-BOS DNA encoding the wild-type or mutated TTR using TransIT-LT-1 (Mirus Corp., Madison, WI). When cells were confluent (90−100%), the medium was changed to serum-free medium, and cells were incubated for another 24 h; then medium was collected for analysis. To examine the effect of T_4 on TTR stabilization, serum-free medium containing 1 μM T_4 was added to the cells. TTR was assayed by Western blotting using the polyclonal anti-human TTR antibody (prealbumin; FL-147; Santa Cruz Biotechnologies, Santa Cruz, CA). Quantification of TTR was accomplished using Image Gauge software (version 4.23; Fujifilm, Japan). The T_4 treatment experiment was performed in triplicate.

Thioflavin T Binding Assay. Wild-type, E54G, and E54K TTRs were incubated with 1 μM T_4 at 37 °C for 3 h in 10 mM phosphate buffer (pH 7.0). After incubation, all samples were mixed with 200 mM acetate buffer (pH 4.1) and incubated at 37 °C for 72 h. TTR samples were prepared to a final concentration of 0.2 mg/mL. Thioflavin T binding assays were performed on 2.5 μg/mL TTR samples by adding freshly prepared 10 μM thioflavin T to 50 mM glycine buffer (pH 9.0). Fluorescence emission spectra were obtained with excitation and emission wavelengths of 450 and 482 nm, respectively. Fluorescence measurements were performed with a F-4500 Hitachi spectrofluorometer (Hitachi, Tokyo, Japan).

Incubation of TTRs with Chloride. TTR samples (0.2 mg/mL) were incubated with various concentrations of KCl (0−1.5 M) in acidic solution adjusted with 10 mM phosphate (pH 7.0) and 200 mM acetate (pH 4.1) buffer containing 1 mM EDTA and 100 mM KCl (final pH 4.4) at 37 °C for 72 h. Amyloid fibril formation was investigated by thioflavin T binding assay.

TTR samples (0.2 mg/mL) were incubated with 1.5 M KCl in 10 mM phosphate (pH 7.0)/1 mM EDTA/1 mM DTT containing 6 M urea at 4 °C for 96 h. After incubation, 5 μg of protein was chemically linked with glutaraldehyde as shown previously (*35*) and subjected to SDS−PAGE. Protein bands were visualized by Coomassie brilliant blue R-250 staining.

RESULTS

Tetramer Formation of Wild-Type TTR and Glu54 TTR Variants. We first examined the quaternary structural stabilities of Glu54 TTR variants. The quaternary structural stability of TTR was determined by the acid-induced tetramer-to-monomer transition assay. In acidic condition, tetramer easily dissociates to monomer. It is widely known that this method can reveal the stability of the tetramer (*36*). Before we performed SDS−PAGE, recombinant TTRs were incubated in phosphate or acetate buffer (pH 3.5−7.0) at 4 °C for 40 h. The fraction of tetramers and monomers at various pHs (pH 3.5−7.0) was calculated as described previously (*15*). The fraction of monomer in the wild-type TTR sample was mostly observed below pH 5.5 (Figure 1A, black squares). As pH increased, the wild-type TTR monomer fraction decreased, with a concomitant increase of tetramer (Figure 1A,B, black squares). E54G TTR showed relatively similar fractions of monomer and tetramer compared with wild-type TTR at pH 3.5−5.5 (Figure 1A,B, green squares), but at pH 6.0−7.0, the monomer fraction of E54G TTR was slightly more than that of wild-type TTR (Figure 1A, green squares), whereas its tetramer fraction was less compared with that of wild-type TTR (Figure 1B, green squares). At pH 5.5−7.0, the amount of monomer in the E54K TTR sample was remarkably higher than that of wild-type TTR (Figure 1A, magenta squares). Consistently, the E54K tetramer fraction at this pH range was less than that of wild-type TTR (Figure 1B, magenta squares), indicating that the tetramer stability of E54K TTR was lower than wild-type TTR.

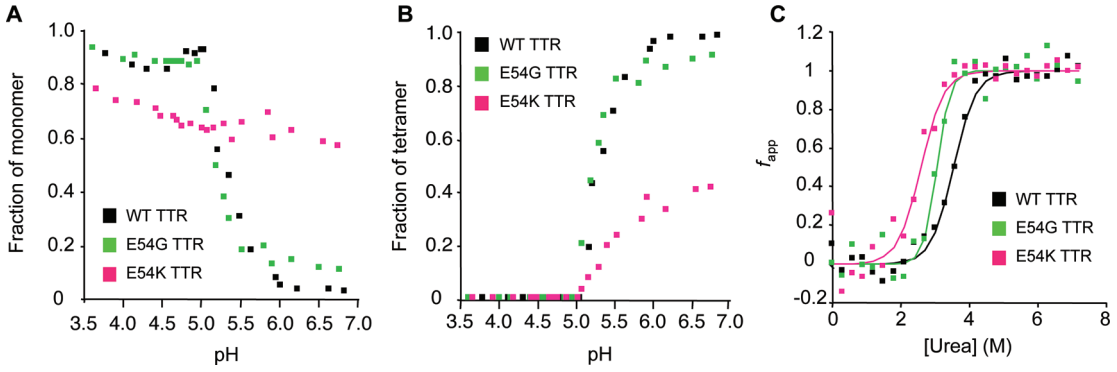

FIGURE 1: Conformation of wild-type and Glu54 variant TTRs. (A, B) Acid-induced tetramer-to-monomer transitions of native recombinant TTR samples; wild-type TTR (black), E54G TTR (green), and E54K TTR (magenta) are shown. The tetramer-to-monomer transitions were monitored by SDS−PAGE, quantified by densitometry, and computed as follows: fractions of monomer ratio/total TTR (A) or fraction of tetramer ratio/total TTR (B). (C) Urea-induced unfolding transition curves of wild-type TTR (black), E54G TTR (green), and E54K TTR (magenta). The unfolding transitions were monitored by CD ellipticity at 215 nm. Using the ellipticity values at 215 nm, we calculated the apparent fractional extent of unfolding, f_{app}, using the equation $f_{app} = (Y_{obs} - Y_N)/(Y_U - Y_N,)$ where Y_N and Y_U represent the baselines for the pre- and posttransition zone, respectively, and Y_{obs} is the observed ellipticity of the protein. The samples were incubated with 0−8 M urea at 25 °C for 96 h before CD measurements.

We next investigated the stability of TTRs by urea-induced denaturation assay (*15*). The apparent fractional extent of unfolding was calculated from values of the CD at 215 nm. The decrease of the CD ellipticity at 215 nm reflects the disruption of secondary structure by urea. The midpoints (C_m) of the urea-induced unfolding curves were obtained after incubation with various concentrations of urea in 50 mM sodium phosphate, 100 mM KCl, and 1 mM ethylenediaminetetraacetic acid (EDTA) (pH 7.0) at 25 °C for 96 h as described previously (*28*). The order of relative stability was wild-type TTR ($C_m = 3.54 \pm 0.04$) > E54G TTR ($C_m = 3.05 \pm 0.04$) > E54K TTR ($C_m = 2.58 \pm 0.06$) (Figure 1C). These data also suggested that Glu54 TTR variants have lower tetramer stability than wild-type TTR.

The Crystal Structure of Glu54 TTR Variants. Because the tetramer formation of Glu54 TTR variants showed obvious difference from that of wild-type TTR in Figure 1, we analyzed and compared the structures of these TTRs by performing X-ray crystallographic studies of recombinant wild-type, E54G, and E54K TTRs (Figure 2A). The crystals of these TTRs belong to space group $P2_12_12$, with two monomers in the asymmetric unit, and diffracted to 2.00, 1.70, and 1.99 Å, respectively. The final refined R values for wild-type, E54G, and E54K TTRs were 16.8%, 20.0%, and 17.2%, respectively (Table 1). The quality of the structures and refinement statistics of wild-type TTR and Glu54 TTR variants are shown in Table 1. Each TTR monomer subunit is composed of 127 amino acids that could be consistently modeled in both monomers, with the exception of the N-terminal residues 1−9 and C-terminal residues 126 and 127, which are highly disordered and lie in regions not defined in the electron density maps as reported previously (*8*). The final model has good geometry, with no residues in disallowed regions of the Ramachandran plot calculated by PROCHECK from the ccp4 program suite (*37*). Each crystal contains one dimer, monomers A and B, in the asymmetric unit (Supporting Information Figure S1A); thus we constructed TTR tetramers using another dimer along the 2-fold axis, symmetric monomers A′ and B′ (Figure 2A and Supporting Information Figure S1B). There was no obvious difference in the overall structure between wild-type and Glu54 TTR variants (Figure 2A). However, the position of residue 54 (shown in color) at the T_4 binding pocket showed a change in the distance between two residues 54 in the dimer−dimer interface (Figure 2A). Moreover, the surface electrostatic potential of residue 54 in Glu54 variants was different from the wild-type TTR tetramer (Figure 2B) and dimer (Supporting Information Figure S2). Comparison of the C^α position of the monomers of wild-type TTR and E54G TTR or E54K TTR showed no differences around β-strand D (Supporting Information Figure S3). The root mean square deviation (rmsd) of C^α between wild-type TTR and E54G TTR of mol A (mol B) is 0.355 Å (0.258 Å). The rmsd of C^α between wild-type TTR and E54K TTR of mol A (mol B) is 0.225 Å (0.169 Å) (Supporting Information Figure S3). These results revealed that although the crystal structures of Glu54 TTR variants have no significant overall structural changes from wild-type TTR and other TTR variants (*9*, *38*), there are differences in the side chain and the surface electrostatic potential around residue 54.

Surface Electrostatic Potential of Wild-Type TTR and Glu54 TTR Variants. The surface electrostatic potential of residue 54 of TTRs determined using the ccp4mg program showed that Glu54 in wild-type, Gly54 in E54G, and Lys54 in E54K TTRs have respectively electronegative, neutral, and electropositive potential (Figure 2B). Consistently, the calculated pK_a values of Lys54 were significantly higher than that of wild-type TTR (Supporting Information Table S1). Interestingly, the p$K_{1/2}$ of Glu54 in wild-type TTR was drastically shifted from its intrinsic pK_a (pK_{int}), suggesting strong interactions of Glu54 with proximal titratable residues, such as Lys15 and His56. A pK_a shift was not observed for Lys54 in E54K TTR (Supporting Information Table S1). Previous studies have suggested that the positively charged Lys15 locus on β-strand A impacts on tetramer stability (*35*). The repulsion of positive charges between Lys15 of two monomers (monomers A, B and monomers A′, B′) destabilizes the tetrameric structure, and it was previously shown that the substitution of Lys15 by Ala15 stabilizes the TTR tetramer (*35*). In wild-type TTR, Glu54, which is electronegative, might be important in stabilizing the edge region around β-strands A and D (Supporting Information Figure S2) by modulating the electropositivity of Lys15. To examine this hypothesis, we investigated the edge region and observed that in wild-type TTR the side chain of Glu54 forms a hydrogen bond with Lys15 and His56 (Figure 3). This interaction might modulate the positive charge of Lys15. In E54G TTR, the direction of the Lys15 side chain shifts toward Gly54 in a manner similar to

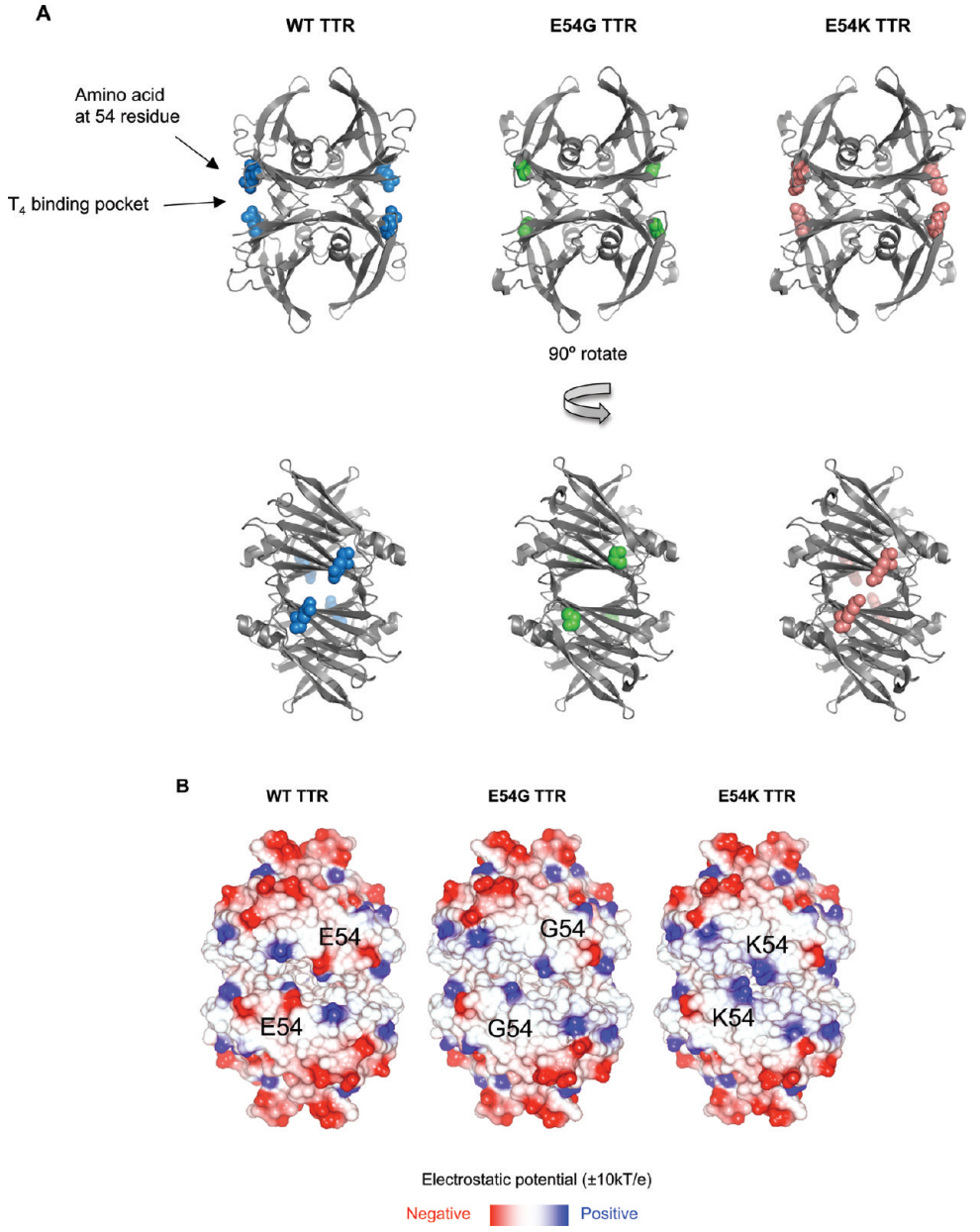

FIGURE 2: Overall structure and surface electrostatic potential of TTR tetramers. (A) The structures of TTRs are drawn with cartoon style. The amino acid residue at position 54 is shown as blue (wild-type TTR), green (E54G TTR), and red (E54K TTR) spheres. (B) The surface electrostatic potentials of TTRs were calculated and drawn with ccp4mg. Positive and negative potentials are shown in blue and red (±10 kT/e), respectively.

wild-type TTR (Figures 3 and Supporting Information Figure S4). Instead of Glu54, the water molecule can mediate the interaction between Ser52 and His56 in E54G TTR (Figure 3). In E54K TTR, the positive charges of Lys15 and Lys54 accumulated in the edge region (Figure 2B and Supporting Information Figure S2), and the side chain of Lys15 shifts to a direction different from that in wild-type and E54G TTRs. Furthermore, the hydrogen bonds that Glu54 forms with Lys15 and with His56 in wild-type TTR are disrupted in E54K TTR (Figure 3). The electron density map around the edge region in E54K TTR shows that the shift in the direction of Lys15 is due to the van der Waals interaction between the side chains of Lys15 and Lys54 (Figure 4). The distances between the side chains of Lys15 in monomer A and monomer A′ (monomer B and monomer B′) in wild-type, E54G, and E54K TTRs are respectively 8.14 (8.73), 9.17 (10.19), and 5.07 (5.92) Å. The shorter distance (in comparison with wild-type) in E54K TTR might induce repulsion between the positively charged Lys15 residues of two monomers.

We next investigated whether the instability of E54K TTR was in part due to the collective positive charges of Lys15 and Lys54. Because it was previously demonstrated that chloride ion suppresses electrical repulsion in the side chain containing Lys15 and stabilizes the tetramer (*35*, *39*), we incubated TTR samples (0.2 mg/mL) with the indicated concentration of KCl at 37 °C and pH 4.4 for 3 days. Amyloid fibril formation was determined by thioflavin T binding assay. At 1 M KCl, amyloid fibril formation was reduced in wild-type TTR (63.93 ± 1.63%) and E54G TTR (70.79 ± 1.86%) but not in E54K TTR (91.35 ± 5.70%) (Figure 5A). The decrease of fibril formation in E54K TTR was observed only at 1.5 M KCl (Figure 5A). This is likely because in E54K TTR Lys54 contributes to the positive charge potential of Lys15; thus the effect of chloride on tetramer stabilization occurred only at higher concentration of KCl. These results correlated with the decrease of monomer fraction and increase of tetramer fraction after urea denaturation in the presence of 1.5 M KCl as determined by SDS−PAGE analysis

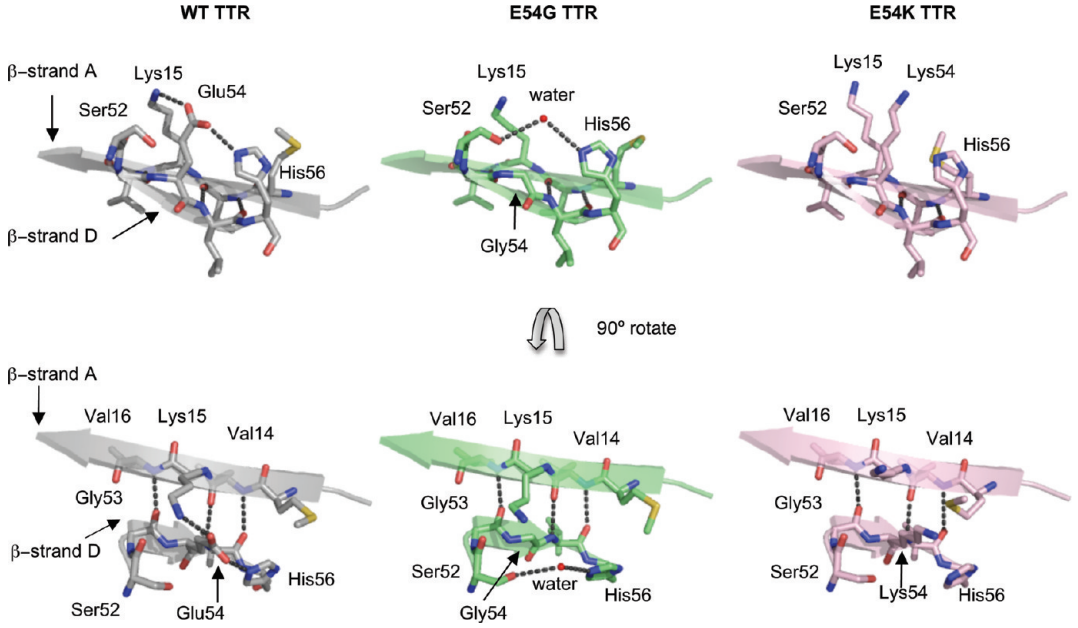

FIGURE 3: Structures of the edge region around β-strands A and D of TTR. β-Strands A and D are shown as cartoon models with carbon atoms in gray (wild-type TTR), green (E54G TTR), and magenta (E54K TTR). Nitrogen, oxygen, and sulfur are in blue, red, and yellow, respectively. Red spheres show the water molecule. Hydrogen bonds are depicted as black dashed lines.

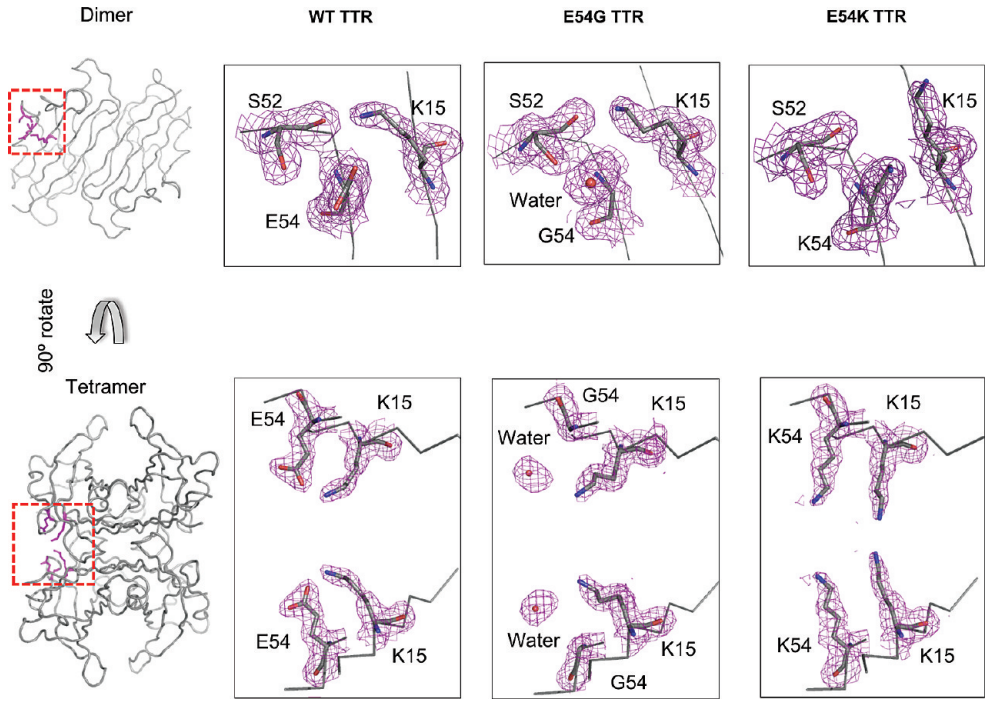

FIGURE 4: $2F_o - F_c$ electron density map showing the direction of Lys15 and the amino acid at position 54. $2F_o - F_c$ electron density map around the edge region of wild-type TTR and Glu54 TTR variants. The $2F_o - F_c$ electron density map is colored purple and was countered at 0.8σ. TTR amino acids at positions 15, 52, and 54 are drawn with lines. Nitrogen and oxygen are shown in blue and red, respectively.

of glutaraldehyde cross-linked samples (Figure 5B). Taken together, these findings suggested that the substitution of Glu54 with Lys residue in E54K TTR impacts on the stability of the tetramer due, in part, to the collective positive charges of Lys15 and Lys54.

Structure of the T_4 Binding Pocket in Glu54 TTR Variants. The physiological function of TTR binding to T_4 contributes to the stabilization of the TTR tetramer and the inhibition of amyloid formation (*13*). Because the Glu54 residue is located at the entrance of the T_4 binding pocket (Figure 2A), we postulated that the mutation in this region might influence the effect of T_4 in Glu54 TTR variants. First, we compared the T_4 binding pocket structure between wild-type TTR and Glu54 TTR variants. The Glu54 mutations did not largely affect the inside structure of the T_4 binding pocket (data not shown). However, the entrance of the T_4 binding pocket was different among the TTRs due to the different length of the amino acid side chain of residue 54 (the distance between C^{α} at residue 54 is almost similar for wild-type TTR and Glu54 TTR variants) (Figure 6; residue 54 is shown in yellow.) In wild-type TTR, the distance between the

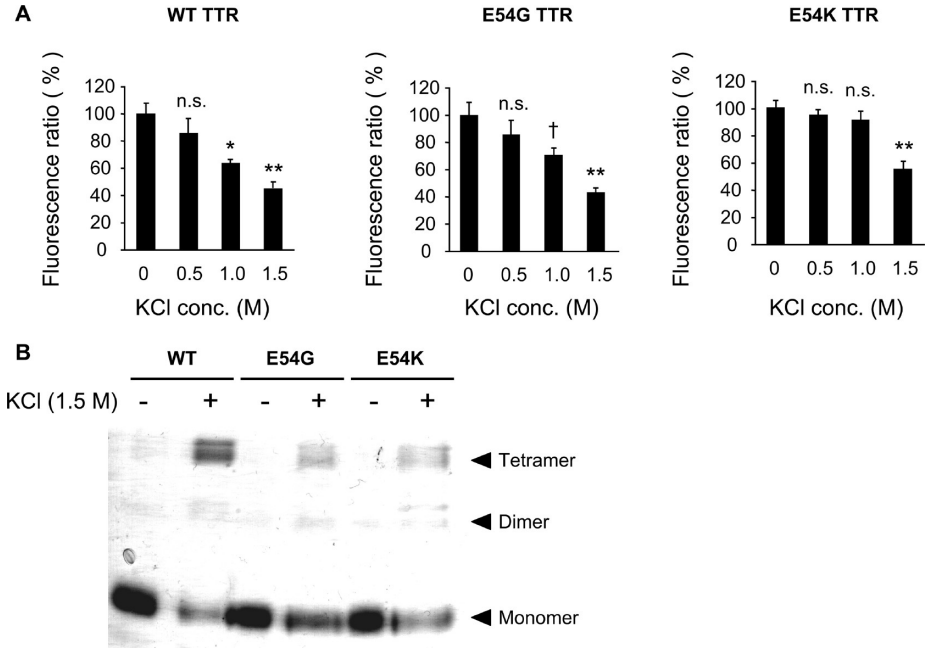

FIGURE 5: Comparison of tetramer stability and amyloid fibril formation in the presence of KCl. (A) TTR fibril formation assays at pH 4.4 with various concentrations of KCl (0−1.5 M) were performed as described in Experimental Procedures. Fluorescence ratio (%) = 100(each concentration of KCl/0 M KCl). Bars shown are representative of three independent experiments. Values represent the mean ± SE. Statistical significance was calculated by the ANOVA (Tukey−Kramer) test (†, $P < 0.1$; *, $P < 0.05$; **, $P < 0.01$). (B) Wild-type TTR and Glu54 TTR variants were incubated with 6 M urea for 96 h in the presence of 1.5 M KCl as described in Experimental Procedures. After incubation, TTR samples were chemically cross-linked with glutaraldehyde and subjected to SDS−PAGE. TTR bands were stained with Coomassie brilliant blue R-250.

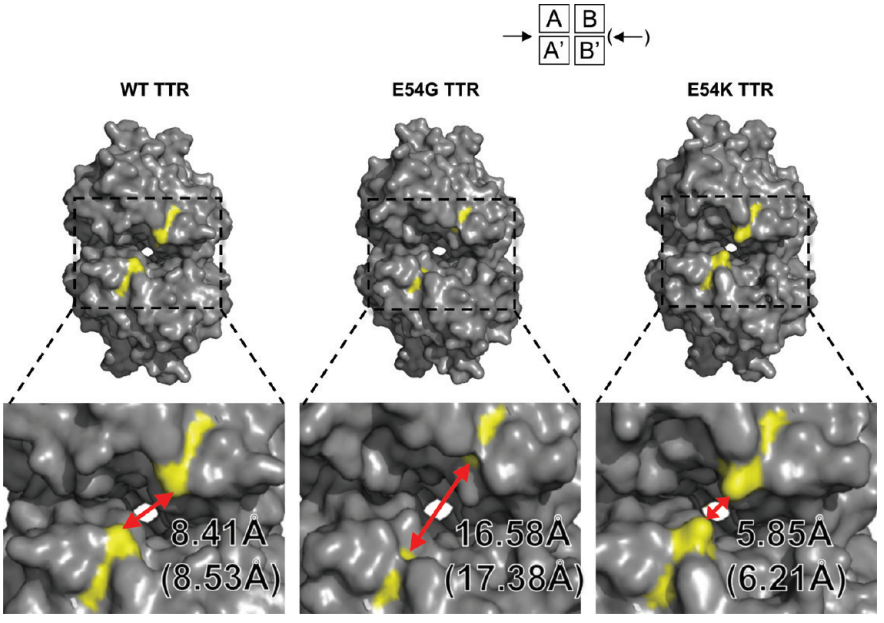

FIGURE 6: Entrance structure of the T_4 binding pocket. The T_4 binding pocket structures of TTRs are shown with surface representation. Lower panels show a close-up view of the entrance structure of the T_4 binding pocket. TTR tetramer and amino acid 54 are in gray and yellow, respectively. The number indicates the distance between amino acid 54 side chains of monomer A and monomer A′ (monomer B and monomer B′).

side chains of Glu54 in monomer A and monomer A′ (monomer B and monomer B′) is 8.41 (8.53) Å. The distance between the side chains of Gly54 in monomer A and monomer A′ (monomer B and monomer B′) of E54G TTR is 16.58 (17.38) Å. The distance between the side chains of Lys54 in monomer A and monomer A′ (monomer B and monomer B′) of E54K TTR is 5.85 (6.21) Å (Figure 6). Therefore, Glu54 mutations generated striking differences in the structure of the entrance of the T_4 binding pocket of Glu54 TTR variants compared with wild-type TTR. The Lys54 mutation in E54K TTR caused the formation of an entrance pocket structure that is smaller than that of the wild-type TTR, and this mutation might interfere with the binding of T_4 to E54K TTR.

Previous study also suggested that Glu54 is crucial for T_4 binding (*12*). However, there is no direct evidence of T_4 binding using Glu54 TTR variants. To determine the affinity of T_4 to

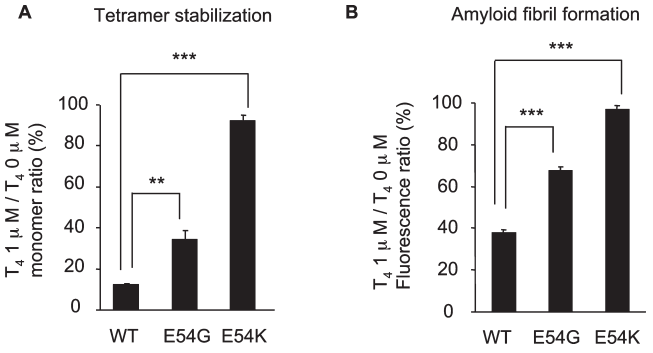

FIGURE 7: Comparison of tetramer stability and amyloid fibril formation of TTRs in the presence of T_4. (A) Western blots of secreted TTR monomer were quantified by densitometric scanning. T_4 1 μM/T_4 0 μM monomer ratio (%) = 100(nonreduced, nonboiled monomer at 1 μM T_4)/(nonreduced, nonboiled monomer at 0 μM T_4). Bars shown are representative of three independent experiments. Values represent the mean ± SE. Statistical significance was calculated by the ANOVA (Tukey−Kramer) test (**, $P < 0.01$; ***, $P < 0.001$). (B) Variant TTRs were incubated for 3 h at 37 °C in 10 mM phosphate buffer at pH 7.0 with or without 1 μM T_4. Then the solution containing TTR was mixed with an equivalent amount of 200 mM acetate buffer at pH 4.1 and incubated for 72 h at 37 °C. Amyloid fibrils of TTR were detected by thioflavin T binding assay. Fluorescence ratio (%) = 100(fluorescence at 1 μM T_4/fluorescence at 0 μM T_4).

these TTRs, we measured the binding rates of T_4 in wild-type and Glu54 TTR variants using automated surface plasmon resonance (SPR) based biosensors Biacore 2000. The dissociation constants (K_d) of Glu54 TTR variants did not significantly differ from that of wild-type TTR (Supporting Information Table S2). However, the rates of association and dissociation (K_{on}, K_{off}) of the Glu54 variants differed notably from wild-type TTR (Supporting Information Table S2). E54G TTR had the highest T_4 association and dissociation rates while E54K TTR showed the lowest T_4 association and dissociation rates among the TTRs (Supporting Information Table S2). These data suggested that the mutation of thhe Glu54 residue in TTR influences the binding and dissociation rates of T_4.

Tetramer Stability and Amyloid Fibril Formation of Glu54 TTR Variants in the Presence of T_4. We next investigated the tetramer stability in the presence of T_4 using the mammalian cell system that we previously developed to monitor the effect of T_4 on TTR stability (*28*). CHO-K1 cells overexpressing the TTR constructs were treated with 1 μM T_4 for 24 h, and the cell media were collected for analysis of the expression of secreted TTRs. The addition of T_4 suppressed the monomer levels of wild-type TTR (12.18 ± 0.76%) in the media as determined by the quantification of the TTR monomer ratio under nonboiled, nonreduced condition (Figure 7A and Supporting Information Figure S5). The monomer level of E54G TTR (34.43 ± 4.34%) was slightly suppressed by T_4 treatment (Figure 7A and Supporting Information Figure S5). In contrast, the monomer level of E54K TTR (92.18 ± 2.56%) was barely suppressed in the presence of T_4 and is significantly higher than that of wild-type and E54G TTRs (Figure 7A and Supporting Information Figure S5).

We also examined the TTR amyloid fibril formation in the presence of T_4. Recombinant wild-type, E54G, and E54K TTRs were incubated at 37 °C for 3 h in 50 mM phosphate buffer (pH 7.0) with or without 1 μM T_4. Then TTR samples were mixed with 200 mM acetate buffer (pH 4.1) and incubated for 72 h. After incubation, production of amyloid fibril was detected by thioflavin T binding assay. Figure 7B showed that the amyloid fibril formation of wild-type TTR was decreased (37.73 ± 1.69%) in the presence of T_4. In agreement with Figure 7A, amyloid formation of Glu54 TTR variants was not effectively suppressed by T_4 treatment compared with wild-type TTR. The fluorescence of E54G and E54K TTRs was 67.81 ± 1.44% and 97.01 ± 1.48%, respectively. In particular, the effect of T_4 was not observed in E54K TTR, indicating a lower affinity of T_4 to E54K TTR compared with wild-type TTR.

DISCUSSION

Extensive studies support the idea that different FAP-associated point mutations lead to differential destabilization of the native protein fold and the formation of amyloid fibrils. Furthermore, it is known that the artificial multiple mutations and deletions in β-strand D (residues Gly53, Glu54, and Leu55) result in significant destabilization of the TTR fold and enhance amyloid fibril formation (*16*). However, the role of naturally occurring single replacement of Glu54 in TTR for tetramer stability, amyloidogenicity, and T_4 binding is less investigated in detail. In this study, we first provided structural insight into the role of Glu54 using two Glu54 TTR variants that are known to cause a clinically aggressive form of FAP. The crystal structures of Glu54 TTR variants are almost identical to wild-type TTR as demonstrated by comparison of rmsd (Supporting Information Figure S3). Moreover, there is no significant difference in hydrogen bond between the main chain of β-strands A and D in these structures. However, we found that side chain interactions and surface electrostatic potential around residue 54 are significantly different between wild-type and Glu54 TTR variants. The Glu54 residue in β-strand D forms the network of hydrogen bonds between the side chain of Lys15−Glu54 and Glu54−His56 in wild-type TTR (Figure 3). Because Lys15−Glu54 interaction could modulate the positive charge of Lys15, the electrostatic repulsion between Lys15 of two monomers (monomer A and monomer A′) is mitigated, which consequently prevents the dissociation of the tetramer. In E54K TTR, due to the van der Waals interaction that exists between the side chains of Lys15 and Lys54, the Lys15 side chain cannot shift similarly as the wild-type TTR (Figures 3 and 4). Moreover, the presence of Lys54 results in the accumulation of positive charges in the edge region as shown by our analysis of the surface electrostatic potential (Figure 2B and Supporting Information Figure S2) and by the chloride experiments (Figure 5A). Glu54−His56 interaction could also stabilize the β-bulge structure composed of residues from Leu55 to Leu58 which is important to stabilize the edge region and reduce amyloidogenesis (*40*). However, the hydrogen bond between Glu54−His56 is disrupted in E54K TTR, and this could destabilize the edge region of E54K TTR (Figure 3). In the case of E54G TTR, the water molecule localizes and mediates the hydrogen bond interaction between Ser52 and His56 (Figure 3). The side chain of Lys15 shifts toward amino acid residue 54 similar to wild-type TTR, suggesting that the absence of a bulky side chain at position 54 may induce a "correct" shift of the Lys15 side chain (Figure 3). However, it is possible that the directional shift of Lys15 in E54G TTR is unstable due to the loss of the Glu54 residue (with its negative charge). Because it has been reported that E54G mutation causes the aggressive form of FAP (*23*), we can speculate that in a physiological environment, i.e., in vivo, E54G TTR tetramer lacks stability. Whether only the Glu residue should occupy

position 54 so as to prevent aggressive FAP remains unclear, but because naturally occurring Glu54 variant TTRs showed clinically aggressive phenotypes, the Glu residue at position 54 is thought to be crucial to prevent amyloidogenesis in vivo.

It has been suggested that the Glu54 residue is crucial for the binding of T_4 to TTR since TTR interacts with T_4 through the carboxylate group of Glu54 (*12*). Our data showing a lower effect of T_4 on Glu54 TTR variants relative to wild-type TTR (Figure 7 and Supporting Information Figure S5) provide evidence on the crucial role of Glu54 in T_4 binding. We observed that the levels of tetramer stability and amyloid fibril formation of E54G TTR were intermediate between those of wild-type and E54K TTRs (Figure 7). This observation might be explained by the fact that T_4 can enter the binding pocket of E54G TTR and may bind to the inner residues in the binding pocket such as Ala108, Ser117, and Thr119 in E54G TTR, but since the rate of T_4 dissociation in E54G TTR was faster than that of wild-type TTR, T_4 binding to E54G TTR may not be as efficient (Supporting Information Table S2). In the case of E54K TTR, the substitution of the Glu54 residue by Lys creates interference in T_4 binding at the entrance of the binding pocket due to the shorter distance (5.85 Å) between the side chains of Lys54 (in monomer A and monomer A′) compared with that of Glu54 (8.41 Å) in wild-type TTR (Figure 6).

On the basis of our data, we conclude that Glu54 in TTR is important for tetramer stability and it influences T_4 binding to TTR. Small molecules have been evaluated for their potential as amyloid fibril inhibitors (*41*). Our study here provides information on the significance of the T_4 binding pocket structure in considering the design of small molecules that bind to the T_4 binding pocket of TTR variants. For some TTR variants that possess mutations capable of compromising the structure around the binding pocket, such as Glu54 TTR variants, small molecules may have to be especially designed to ensure high-affinity binding.

SUPPORTING INFORMATION AVAILABLE

A figure illustrating the structure of TTR tetramer and dimer, a figure showing the surface electrostatic potentials of TTR dimers, figures illustrating the superimposition of TTR monomers and of the edge region of TTRs (wild type and Glu54 variants), a figure showing the dose-dependent effect of T_4 on the level of TTR monomers in the culture media, a table containing the computed pK_a values of the TTRs, and a table containing the kinetic constants of T_4 binding to TTRs. This material is available free of charge via the Internet at http://pubs.acs.org.

REFERENCES

1. Ando, Y., Araki, S., and Ando, M. (1993) Transthyretin and familial amyloidotic polyneuropathy. *Intern. Med. 32*, 920–922.
2. Sato, T., Ando, Y., Susuki, S., Mikami, F., Ikemizu, S., Nakamura, M., Suhr, O., Anraku, M., Kai, T., Suico, M. A., Shuto, T., Mizuguchi, M., Yamagata, Y., and Kai, H. (2006) Chromium(III) ion and thyroxine cooperate to stabilize the transthyretin tetramer and suppress in vitro amyloid fibril formation. *FEBS Lett. 580*, 491–496.
3. Noy, N., Slosberg, E., and Scarlata, S. (1992) Interactions of retinol with binding proteins: studies with retinol-binding protein and with transthyretin. *Biochemistry 31*, 11118–11124.
4. Monaco, H. L., Mancia, F., Rizzi, M., and Coda, A. (1994) Crystallization of the macromolecular complex transthyretin-retinol-binding protein. *J. Mol. Biol. 244*, 110–113.
5. Monaco, H. L., Rizzi, M., and Coda, A. (1995) Structure of a complex of two plasma proteins: transthyretin and retinol-binding protein. *Science 268*, 1039–1041.
6. Wojtczak, A. (1997) Crystal structure of rat transthyretin at 2.5 Å resolution: first report on a unique tetrameric structure. *Acta Biochim. Pol. 44*, 505–517.
7. Sebastiao, M. P., Saraiva, M. J., and Damas, A. M. (1998) The crystal structure of amyloidogenic Leu55→Pro transthyretin variant reveals a possible pathway for transthyretin polymerization into amyloid fibrils. *J. Biol. Chem. 273*, 24715–24722.
8. Steinrauf, L. K., Hamilton, J. A., Braden, B. C., Murrell, J. R., and Benson, M. D. (1993) X-ray crystal structure of the Ala-109→Thr variant of human transthyretin which produces euthyroid hyperthyroxinemia. *J. Biol. Chem. 268*, 2425–2430.
9. Terry, C. J., Damas, A. M., Oliveira, P., Saraiva, M. J., Alves, I. L., Costa, P. P., Matias, P. M., Sakaki, Y., and Blake, C. C. (1993) Structure of Met30 variant of transthyretin and its amyloidogenic implications. *EMBO J. 12*, 735–741.
10. Ciszak, E., Cody, V., and Luft, J. R. (1992) Crystal structure determination at 2.3-Å resolution of human transthyretin-3′,5′-dibromo-2′,4,4′,6-tetrahydroxyaurone complex. *Proc. Natl. Acad. Sci. U.S.A. 89*, 6644–6648.
11. Hamilton, J. A., Steinrauf, L. K., Liepnieks, J., Benson, M. D., Holmgren, G., Sandgren, O., and Steen, L. (1992) Alteration in molecular structure which results in disease: the Met-30 variant of human plasma transthyretin. *Biochim. Biophys. Acta 1139*, 9–16.
12. Wojtczak, A., Cody, V., Luft, J. R., and Pangborn, W. (1996) Structures of human transthyretin complexed with thyroxine at 2.0 Å resolution and 3′,5′-dinitro-N-acetyl-L-thyronine at 2.2 Å resolution. *Acta Crystallogr., Sect. D: Biol. Crystallogr. 52*, 758–765.
13. Miroy, G. J., Lai, Z., Lashuel, H. A., Peterson, S. A., Strang, C., and Kelly, J. W. (1996) Inhibiting transthyretin amyloid fibril formation via protein stabilization. *Proc. Natl. Acad. Sci. U.S.A. 93*, 15051–15056.
14. Bryson, D. I., Doctor, N., Johnson, R., Baranov, S., and Haddy, A. (2005) Characteristics of iodide activation and inhibition of oxygen evolution by photosystem II. *Biochemistry 44*, 7354–7360.
15. Takeuchi, M., Mizuguchi, M., Kouno, T., Shinohara, Y., Aizawa, T., Demura, M., Mori, Y., Shinoda, H., and Kawano, K. (2007) Destabilization of transthyretin by pathogenic mutations in the DE loop. *Proteins 66*, 716–725.
16. Goldsteins, G., Andersson, K., Olofsson, A., Dacklin, I., Edvinsson, A., Baranov, V., Sandgren, O., Thylen, C., Hammarstrom, S., and Lundgren, E. (1997) Characterization of two highly amyloidogenic mutants of transthyretin. *Biochemistry 36*, 5346–5352.
17. Yamamoto, K., Hsu, S. P., Yoshida, K., Ikeda, S., Nakazato, M., Shiomi, K., Cheng, S. Y., Furihata, K., Ueno, I., and Yanagisawa, N. (1994) Familial amyloid polyneuropathy in Taiwan: identification of transthyretin variant (Leu55→Pro). *Muscle Nerve 17*, 637–641.
18. Liu, K., Kelly, J. W., and Wemmer, D. E. (2002) Native state hydrogen exchange study of suppressor and pathogenic variants of transthyretin. *J. Mol. Biol. 320*, 821–832.
19. Liu, K., Cho, H. S., Hoyt, D. W., Nguyen, T. N., Olds, P., Kelly, J. W., and Wemmer, D. E. (2000) Deuterium-proton exchange on the native wild-type transthyretin tetramer identifies the stable core of the individual subunits and indicates mobility at the subunit interface. *J. Mol. Biol. 303*, 555–565.
20. Togashi, S., Watanabe, H., Nagasaka, T., Shindo, K., Shiozawa, Z., Maeda, S., Tawata, M., and Onaya, T. (1999) An aggressive familial amyloidotic polyneuropathy caused by a new variant transthyretin Lys 54. *Neurology 53*, 637–639.
21. Reilly, M. M., Adams, D., Booth, D. R., Davis, M. B., Said, G., Laubriat-Bianchin, M., Pepys, M. B., Thomas, P. K., and Harding, A. E. (1995) Transthyretin gene analysis in European patients with suspected familial amyloid polyneuropathy. *Brain 118* (Part 4), 849–856.
22. Busse, A., Sanchez, M. A., Monterroso, V., Alvarado, M. V., and Leon, P. (2004) A severe form of amyloidotic polyneuropathy in a Costa Rican family with a rare transthyretin mutation (Glu54Lys). *Am. J. Med. Genet. A 128A*, 190–194.
23. Kim, H. S., Kim, S. M., Kang, S. W., Jung, S. C., Lee, K. S., Kim, T. S., and Choi, Y. C. (2005) An aggressive form of familial amyloid polyneuropathy caused by a Glu54Gly mutation in the transthyretin gene. *Eur. J. Neurol. 12*, 657–659.
24. Kelly, J. W., Colon, W., Lai, Z., Lashuel, H. A., McCulloch, J., McCutchen, S. L., Miroy, G. J., and Peterson, S. A. (1997) Transthyretin quaternary and tertiary structural changes facilitate misassembly into amyloid. *Adv. Protein Chem. 50*, 161–181.
25. Neumann, P., Cody, V., and Wojtczak, A. (2005) Ligand binding at the transthyretin dimer-dimer interface: structure of the transthyretin-T4Ac complex at 2.2 angstrom resolution. *Acta Crystallogr., Sect. D: Biol. Crystallogr. 61*, 1313–1319.

26. Wojtczak, A., Neumann, P., and Cody, V. (2001) Structure of a new polymorphic monoclinic form of human transthyretin at 3 A resolution reveals a mixed complex between unliganded and T4-bound tetramers of TTR. *Acta Crystallogr., Sect. D: Biol. Crystallogr. 57*, 957–967.
27. Klabunde, T., Petrassi, H. M., Oza, V. B., Raman, P., Kelly, J. W., and Sacchettini, J. C. (2000) Rational design of potent human transthyretin amyloid disease inhibitors. *Nat. Struct. Biol. 7*, 312–321.
28. Sato, T., Susuki, S., Suico, M. A., Miyata, M., Ando, Y., Mizuguchi, M., Takeuchi, M., Dobashi, M., Shuto, T., and Kai, H. (2007) Endoplasmic reticulum quality control regulates the fate of transthyretin variants in the cell. *EMBO J. 26*, 2501–2512.
29. Shinohara, Y., Mizuguchi, M., Matsubara, K., Takeuchi, M., Matsuura, A., Aoki, T., Igarashi, K., Nagadome, H., Terada, Y., and Kawano, K. (2003) Biophysical analyses of the transthyretin variants, Tyr114His and Tyr116Ser, associated with familial amyloidotic polyneuropathy. *Biochemistry 42*, 15053–15060.
30. Peterson, S. A., Klabunde, T., Lashuel, H. A., Purkey, H., Sacchettini, J. C., and Kelly, J. W. (1998) Inhibiting transthyretin conformational changes that lead to amyloid fibril formation. *Proc. Natl. Acad. Sci. U.S.A. 95*, 12956–12960.
31. Brunger, A. T., Adams, P. D., Clore, G. M., DeLano, W. L., Gros, P., Grosse-Kunstleve, R. W., Jiang, J. S., Kuszewski, J., Nilges, M., Pannu, N. S., Read, R. J., Rice, L. M., Simonson, T., and Warren, G. L. (1998) Crystallography & NMR system: A new software suite for macromolecular structure determination. *Acta Crystallogr., Sect. D: Biol. Crystallogr. 54*, 905–921.
32. Emsley, P., and Cowtan, K. (2004) Coot: model-building tools for molecular graphics. *Acta Crystallogr., Sect. D: Biol. Crystallogr. 60*, 2126–2132.
33. Winn, M. D., Murshudov, G. N., and Papiz, M. Z. (2003) Macromolecular TLS refinement in REFMAC at moderate resolutions. *Methods Enzymol. 374*, 300–321.
34. Potterton, L., McNicholas, S., Krissinel, E., Gruber, J., Cowtan, K., Emsley, P., Murshudov, G. N., Cohen, S., Perrakis, A., and Noble, M. (2004) Developments in the CCP4 molecular-graphics project. *Acta Crystallogr., Sect. D: Biol. Crystallogr. 60*, 2288–2294.
35. Hammarstrom, P., Jiang, X., Deechongkit, S., and Kelly, J. W. (2001) Anion shielding of electrostatic repulsions in transthyretin modulates stability and amyloidosis: insight into the chaotrope unfolding dichotomy. *Biochemistry 40*, 11453–11459.
36. Lai, Z., Colon, W., and Kelly, J. W. (1996) The acid-mediated denaturation pathway of transthyretin yields a conformational intermediate that can self-assemble into amyloid. *Biochemistry 35*, 6470–6482.
37. Potterton, E., Briggs, P., Turkenburg, M., and Dodson, E. (2003) A graphical user interface to the CCP4 program suite. *Acta Crystallogr., Sect. D: Bio. Crystallogr. 59*, 1131–1137.
38. Neto-Silva, R. M., Macedo-Ribeiro, S., Pereira, P. J., Coll, M., Saraiva, M. J., and Damas, A. M. (2005) X-ray crystallographic studies of two transthyretin variants: further insights into amyloidogenesis. *Acta Crystallogr., Sect. D: Biol. Crystallogr. 61*, 333–339.
39. Hornberg, A., Hultdin, U. W., Olofsson, A., and Sauer-Eriksson, A. E. (2005) The effect of iodide and chloride on transthyretin structure and stability. *Biochemistry 44*, 9290–9299.
40. Eneqvist, T., Andersson, K., Olofsson, A., Lundgren, E., and Sauer-Eriksson, A. E. (2000) The beta-slip: a novel concept in transthyretin amyloidosis. *Mol. Cell 6*, 1207–1218.
41. Miller, S. R., Sekijima, Y., and Kelly, J. W. (2004) Native state stabilization by NSAIDs inhibits transthyretin amyloidogenesis from the most common familial disease variants. *Lab. Invest. 84*, 545–552.